Asymmetric hydrogenation using Wilkinson-type rhodium complexes immobilized onto mesoporous silica†

Reine Sayah,[a,b] Eric Framery*[b] and Véronique Dufaud*[a]

Received 17th May 2009, Accepted 30th July 2009
First published as an Advance Article on the web 19th August 2009
DOI: 10.1039/b915563p

Heterogeneous chiral catalysts based on the DIOP-Rh system were prepared by covalent immobilization onto SBA type silicas using two different strategies. In the first route, a chiral analogue of Wilkinson's catalyst, [Rh(diop)($PPh_2(CH_2)_2Si(OCH_2CH_3)_3$)Cl], **2**, was immobilized onto a SBA-15 surface *via* a classical post-grafting procedure affording **[2]/SBA-15**. The covalent link to the surface was introduced through the monodentate phosphine ligand while keeping the structure of the chiral directing group intact. The second approach involved a two step synthesis: achiral $RhCl\{PPh_2(CH_2)_2Si(OCH_2CH_3)_3\}_3$, **3**, was first integrated within the walls of the silica framework during the synthesis of the oxide followed by incorporation of the chiral auxiliary in the pores of the material by post-synthetic grafting of a siloxane-containing DIOP ligand, **4**. This led initially to the formation of **[3][4]@PMOs** in which stereogenic and reactive centers are not directly linked together but are in close proximity within a confined space. For characterisation, both molecular and solid state techniques were used to determine the structural and textural properties of the hybrid materials. The catalytic performances of the materials was evaluated using the hydrogenation of methyl (*Z*)-2-*N*-acetylaminocinnamate. Generally, the **[2]/SBA-15** catalyst leads to full, selective conversion with an ee of 57% in favor of the (*R*)-enantiomer. These data compare favorably to those reported for homogeneous counterparts. Rate of hydrogenation was further improved by varying the reaction parameters (temperature and pressure) or by generating *in situ* cationic active site just prior to the catalysis. In the case of **[3][4]@PMOs**, lower conversions were achieved (15 to 41%), which is attributed to restricted accessibility to the rhodium centre. Enantioinduction up to 26% was observed for these systems. Catalyst recycling was studied for **[2]/SBA-15** and it was shown that the catalyst could be re-used several times without loss of enantioselectivity or activity.

Introduction

Homogeneous catalyzed asymmetric hydrogenation is certainly the most widely used industrial reaction and has been applied, over the years, to a broad scope of prochiral precursors such as enamides, itaconates, arylketones, propenoic acids and β-ketoesters.[1] For example, in the pharmaceutical industry, the Monsanto process for the preparation of the amino acid L-dopa has attracted considerable attention from both academic and industrial researchers.[2] Chiral C_2-symmetric diphosphines, such as DIOP,[3] DIPAMP,[4] Chiraphos,[5] DuPhos[6] and BINAP,[7] are probably the best ligands for the rhodium asymmetric hydrogenation of these compounds, providing high enantioselectivity.

Although, high activity and better control of stereoselectivity are generally easier to achieve with homogeneous systems, traditional homogeneous catalysis presents major problems in terms of product purification and separation of expensive metal catalyst that leads to toxic wastes. These problems are particularly important when dealing with large scale-synthesis for environmental and economic concerns. Immobilized catalysts have been developed to avoid such drawbacks and various methodologies are available to heterogenize homogeneous catalysts onto organic or inorganic carriers: entrapment, adsorption, ion-pair formation and covalent binding.[8] There are several examples of noncovalent anchoring of ligands or catalysts which associate rhodium diphosphines with silica or modified silica matrix[9] using the ion-exchange strategy pioneered by Augustine *et al.*[10] Typically, ionic transition-metal complexes are immobilized onto a negatively charged silica surface such as Al-MCM-41,[9b,9c] and AlTUD-1[9d] or through the use of heteropoly acids as the anchor,[10] affording relatively stable and effective catalysts, although these catalysts are generally less enantioselective than their soluble counterparts.

The covalent binding approach remains, however, the most employed method of heterogenization of enantioselective catalysts providing many advantages such as the reduction of

[a]*Laboratoire de Chimie, UMR 5182 ENS/CNRS, Ecole Normale Supérieure de Lyon, 46 allée d'Italie, F-69364 Lyon Cedex 07, France. E-mail: vdufaud@ens-lyon.fr; Fax: +33 4727 28860; Tel: +33 4727 28857*
[b]*ICBMS, UMR-CNRS 5246, Equipe Synthèse Asymétrique, Université de Lyon, Université Lyon 1, 43 boulevard du 11 Novembre, 1918, F-69622, Villeurbanne cedex, France. E-mail: framery@univ-lyon1.fr; Fax: +33 4724 48160; Tel: +33 4724 46263*
† Electronic supplementary information (ESI) available: Fig. S1–S6. See DOI: 10.1039/b915563p

leaching and metal contamination of the products. To our knowledge, there are few examples of chiral bis-phosphines anchored to mesoporous silica support with a covalent bond, probably due to time-consuming and not always predictable effects of ligand replacement on activity and selectivity of the ligand modification. In 2000, S. A. Raynor *et al.*[11] reported a chiral Pd-catalyst derived from 1,1′-bis(diphenylphosphino)ferrocene covalently anchored to the surface of MCM-41 type silica for which a beneficial effect due to catalyst confinement was demonstrated. In a 2001 report, C. M. Crudden *et al.*[12] showed the importance of the use of an inert spacer $EtSi(OEt)_3$ in order to prevent the formation of P(V) species, when an achiral bidentate rhodium phosphine complex was linked to the surface of SBA-15 silica. More recently, chiral bisphosphine-based ligands such as Meo-Biphep, Biphemp, and BINAP have been supported on various inorganic oxides, like the commercially available silica gel (Grace 332),[13] or on a silica presenting a high pore volume and a low surface area.[14] In the latter report, BINAP-supported Ru- and Rh-catalysts gave similar activity and selectivity to the homogeneous catalyst for the hydrogenation of enamides and β-ketoesters. However, no recycling was possible with the Rh-catalyst due to the low stability of the complex, while the Ru-catalyst was recycled 5 times without loss of activity and enantioselectivity in the hydrogenation of methyl 3-oxobutanoate.

Here, we report on the synthesis and thorough characterization of covalently immobilized DIOP-rhodium complexes onto SBA type silicas. The first type of catalyst was a chiral analogue of Wilkinson's catalyst, $[Rh(diop)(PPh_2(CH_2)_2Si(OCH_2CH_3)_3)Cl]$, which was grafted onto the surface of SBA-15 silica *via* a monophosphine anchor. The hybrid material was further modified by passivation of the surface and by *in situ* generation of the cationic analogue of the initial neutral rhodium complex. In order to address the question of the proximity between the substrate, the chiral auxiliary and the reactive centre, a hybrid material was prepared *via* an unconventional approach wherein an achiral $RhCl\{PPh_2(CH_2)_2Si(OCH_2CH_3)_3\}_3$ was first integrated within the walls of the silica framework during the synthesis of the oxide followed by incorporation of the chiral directing group in the pores of the material by post-grafting a siloxane-containing DIOP ligand. The performances of these catalytic hybrids were then examined in the hydrogenation of methyl (*Z*)-2-*N*-acetylaminocinnamate. The recycling of the first type of immobilized catalyst was also studied.

Results and discussion

Synthesis of molecular rhodium precursor and hybrid materials

Dealing with covalent anchoring of homogeneous asymmetric catalysts usually implies the chemical modification of the chiral ligand, which in turn often leads to the loss of chiral induction. In our approach, we chose to incorporate the covalent link to the surface not through the chiral directing group but rather through another monodentate phosphine ligand. In this manner, the structure of the DIOP ligand and particularly its rigidity, which controls the stereoselectivity, were kept intact. The chiral analogue of Wilkinson's catalyst bearing siloxane moities was prepared in quantitative yield *via* a one pot reaction involving first the cleavage of the chloride bridges in $[Rh(COD)Cl]_2$ with two equivalents of $PPh_2(CH_2)_2Si(OCH_2CH_3)_3$ followed by the substitution of the remaining COD ligand by DIOP (Scheme 1), leading to a rhodium complex $[Rh(diop)(PPh_2(CH_2)_2Si(OCH_2CH_3)_3)Cl]$, **2**, which associates a silylated monodentate phosphine, a chiral bidentate DIOP and a chloro ligand in a pseudo-square planar arrangement. The ^{31}P NMR spectra (ESI, Fig. S1 and Fig. S2)† are in good accord with the data reported by H. Brunner *et al.* for similar chiral rhodium complexes.[15] In particular, the ^{31}P NMR spectrum of **2** (ESI, Fig. S2)† was characterized by the presence of three sets of signals, each of which being split into 8 lines (doublets of doublets of doublets) ascribed to the coupling of one P atom with the other two phosphorus atoms and the rhodium atom. Note this pattern indicated that the two P atoms of the chiral C_2-symmetric diphosphine in **2** are inequivalent.

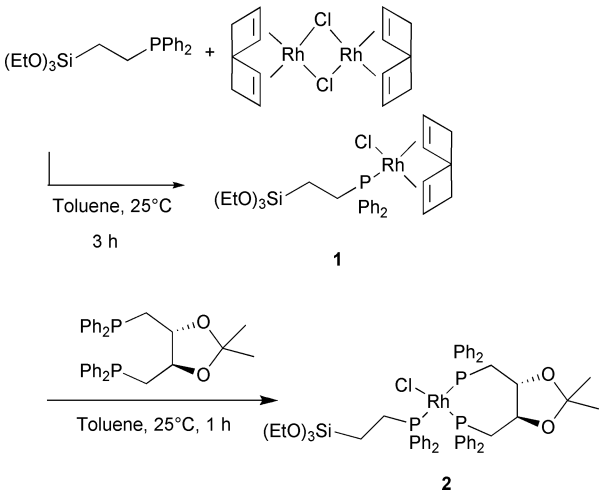

Scheme 1 Synthesis of Wilkinson-type chiral catalyst **2**.

The corresponding hybrid material referred to as **[2]/SBA-15** was produced by post-synthetic modification of a preformed mesoporous SBA-15 type silica with **2** in toluene at 65 °C through condensation of surface silanols with the siloxane groups of **2** (Scheme 2). The SBA-15 silica was chosen not only for the general properties of mesostructured materials (high surface area, well ordered pore arrays, uniform pore size distribution), but more specifically for its large pore volume and diameter (up to 80 Å) which would allow faster diffusion of guest molecules. In some case, the silica surface was further passivated using $(CH_3)_3SiCl$ as silylating agent (resulting in material **[2S]/SBA-15**), in order to avoid complications due to residual surface silanols in later steps.

Several methods were used to characterize the molecular and bulk properties of the catalytic solids: X-ray powder diffraction at small angles, elemental analysis, thermogravimetric analysis, infrared spectroscopy, diffuse reflectance UV-Visible spectroscopy, multi-nuclear NMR spectroscopy and nitrogen sorptions. The physicochemical properties of the hybrid materials derived from the PXRD and sorption analyses are summarized in Table 1. Small angle powder XRD patterns of SBA-15 materials were collected before and after grafting of **2**

Table 1 Physical and textural properties of rhodium containing hybrid silica materials

			Structural and textural properties							
Sample	Rh%$_{wt}$	P%$_{wt}$	d_{100} (Å)[a]	a_0 (Å)[b]	Wall thickness (Å)[c]	V_μ ($cm^3.g^{-1}$)[d]	V_p ($cm^3.g^{-1}$)[e]	D_p (Å)	S_{BET} ($m^2.g^{-1}$)	C_{BET}
SBA-15	—	—	98	114	45	0.04	1.05	69[f]	804	130
[2]/SBA-15	2.4	2.5	102	118	60	0.02	0.49	58[f]	320	85
[3]@PMOs	0.8	0.9	34	39	17	0.36	0.44	22[g]	1030	25
[3][4]@PMOs	0.8	1.2	34	39	21	0.28	0.33	18[g]	800	28

[a] d(100) spacing; [b] $a_0 = 2d(100)/\sqrt{3}$, hexagonal lattice parameter calculated from XRD; [c] calculated by a_0–pore size; [d] micropore volume determined using the t-plot method; [e] total pore volume at $P/P_0 = 0.980$; [f] pore size applying the BJH pore analysis; [g] pore size applying the BdB pore analysis.

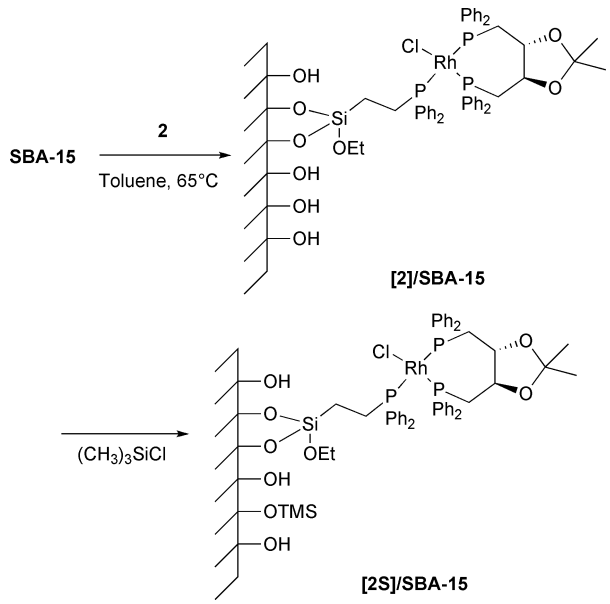

Scheme 2 Grafting of chiral rhodium complex **2** onto SBA-15 silica material.

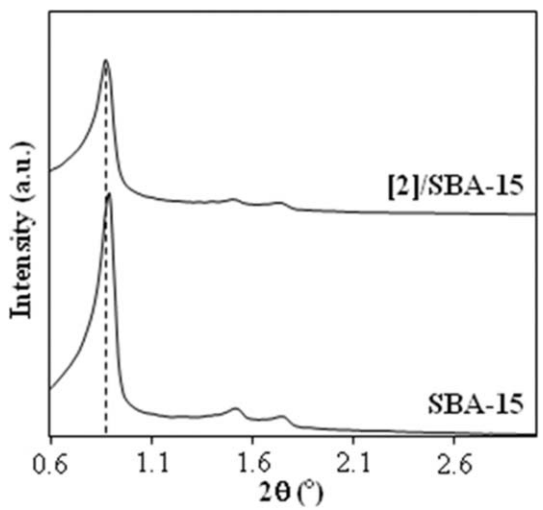

Fig. 1 X-Ray powder diffraction pattern of the SBA-15 material after grafting of **2**.

and are presented in Fig. 1. Three well-resolved peaks in the 2θ-range of 0.6-3° that correspond to (100), (110) and (200) reflections were observed for the parent and rhodium modified silica materials, indicating that the chemical bonding procedure did not diminish the structural long-range ordering of the solid.

After grafting of **2**, a slight decrease in intensity of the d_{100} reflection along with an increase of the unit cell parameter from 114 Å for calcined **SBA-15** to 118 Å for **[2]/SBA-15** was noted (Table 1). This latter variation could be attributed either to a change in the wall thickness or to a modification of the pore size (*vide infra*). Nitrogen adsorption-desorption measurements for **[2]/SBA-15** and parent **SBA-15** silica show a type IV isotherm typical of mesoporous solids (Fig. 2). A well defined sharp inflexion at a relative pressure range of 0.6 to 0.8 P/P0 was shown for both solids, although a decrease in N_2 uptake was observed for **[2]/SBA-15** consistent with the presence of a bulky organometallic complex in the pore channels. Relatively narrow pore diameter distributions were obtained for both materials, with a median pore diameter varying from 69 to 58 Å upon functionalization (Table 1).

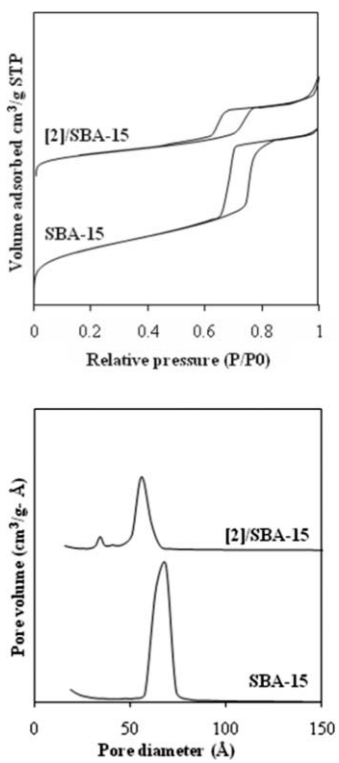

Fig. 2 Nitrogen adsorption/desorption isotherms and pore size distribution of calcined SBA-15 silica before and after the grafting of **2**.

Note that the decrease in pore size was accompanied by a significant increase in the wall thickness (from 45 to 60 Å). The grafting of **2** resulted also in a sharp decrease in the BET surface

area (from 804 m^2g^{-1} to 320 m^2g^{-1}, Table 1) and the pore volume (from 1.05 cm^3g^{-1} to 0.49 cm^3g^{-1}, Table 1). Taken together, these data suggest that a significant amount of rhodium complex was immobilized within the pores of the silica framework. This was confirmed by quantitative determination of organic and metal contents using thermogravimetric and elemental analyses (Table 1, Figure S3 in ESI).† Elemental analysis showed that **[2]/SBA-15** contained on average three phosphorus atoms (presumably one DIOP ligand and one monophosphine ligand) per rhodium atom (2.4%$_{wt}$ Rh and 2.5%$_{wt}$ P) indicating that the integrity of the molecular precursor **2** was basically maintained throughout the grafting procedure. TGA for **[2]/SBA-15** carried out under flowing air was characterized by three weight loss regions (Figure S3).† A first weight loss of less than 4.1% was observed below 200 °C caused by the desorption of physisorbed water. The weight loss of 15.2% centered at 407 °C arose from the decomposition of the organometallic and organic species. For the purpose of reporting organic content, the weight loss between 200 and 600 °C was taken as an estimate of the total amount of the organics. Thus, the functional group loading for **[2]/SBA-15** hybrid was found to be 0.19 g/g of dry SiO_2.[16] Weight loss above 600 °C was presumably due to the condensation of surface silanols and loss of H_2O.

Solid state ^{29}Si NMR provides further information about the silicon environment and the nature of the link with the silica surface. The ^{29}Si CP-MAS NMR spectrum of **[2]/SBA-15** (Fig. 3) displayed three distinct peaks in the -90 to -110 ppm spectral region ascribed to Q^2, Q^3 and Q^4 silicon resonances typical of the silica network. Also, one observes the presence of a broad resonance centered at -65 ppm assigned to *T*-type silicates, that is, the silicon attached to alkyl linkages of $PPh_2(CH_2)_2Si(OCH_2CH_3)_3$ at the surface of the support which is a clear indication that the monophosphine ligand is covalently bound to the support. The MAS ^{31}P NMR spectrum of **[2]/SBA-15** shown in Fig. 4 exhibited one broad resonance centered at 35 ppm attributed to rhodium coordinated phosphorous atoms along with spinning side bands. The width of the signal, however, prevented an accurate determination of the Rh-P coupling constants as well rendering impossible the observation of the inequivalence of the three phosphorus atoms.

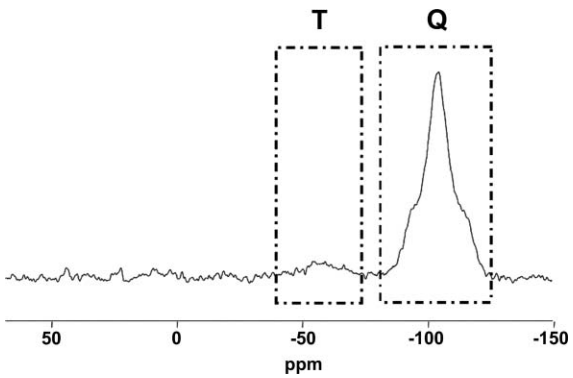

Fig. 3 CP-MAS ^{29}Si NMR of **[2]/SBA-15**.

The question of the proximity between the substrate, the chiral auxiliary and the reactive centre is of crucial importance to achieve chiral transition state and thus high enantioinduction. To address this point, we prepared a new type of chiral hybrid material in which the metallic center and the chiral directing group are not linked together but rather placed in different microenvironments within the catalytic solid. One of us has recently reported on a novel synthesis of active heterogeneous hydrogenation catalysts consisting of organophosphino rhodium complexes covalently incorporated inside the pore walls of mesostructured porous silica.[17] This surfactant-directed assembly approach was shown to maintain the active-site integrity and chemical environment while minimizing pore blockage and distribution inhomogeneity that is a frequent consequence of post-synthesis grafting. The strategy followed here involved a two step synthesis as depicted in Scheme 3. The first step corresponds to the direct incorporation of a Wilkinson-type complex having multiple points of attachment, $RhCl\{PPh_2(CH_2)_2Si(OCH_2CH_3)_3\}_3$, **3**, as an integral part of the mesoporous framework affording achiral hybrid solid **[3]@PMOs**. After stabilizing the mesostructure through silylation followed by template removal, subsequent functionalization of the pores was achieved by reacting a DIOP derived ligand, (2S,3S)-1,4-bis(diphenylphosphino)butane-2,3-diyl-bis[(3-triethoxysilyl) propyl)carbamate],[18] **4**, with residual silanols yielding a new chiral solid referred to as **[3][4]@PMOs**.

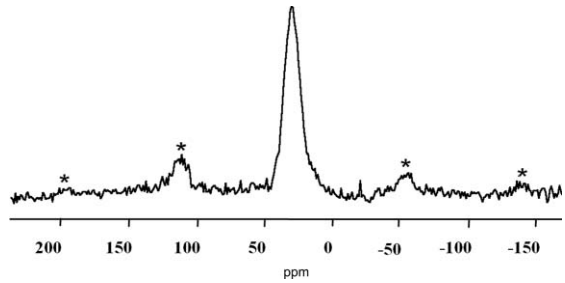

Fig. 4 MAS ^{31}P NMR of **[2]/SBA-15**. The * denote spinning side bands.

The state of the solid structure and the integrity of the molecular complex were characterized at each major step of elaboration by several analytical and spectroscopic methods.

Physicochemical and textural property data are included in Table 1. The X-ray diffraction (XRD) powder pattern of **[3][4]@PMOs** (Fig. 5) showed that mesoscopic order was maintained in the final material. The intense diffraction peak in the 2θ-range of 1 to 10°, along with weak higher order reflexion are characteristic of hexagonally ordered mesophases, with a

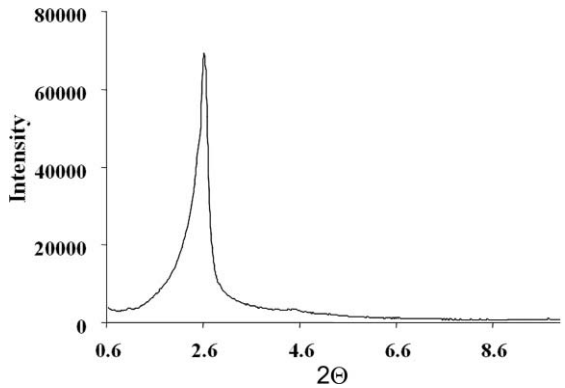

Fig. 5 X-Ray powder diffraction pattern of **[3][4]@PMOs**.

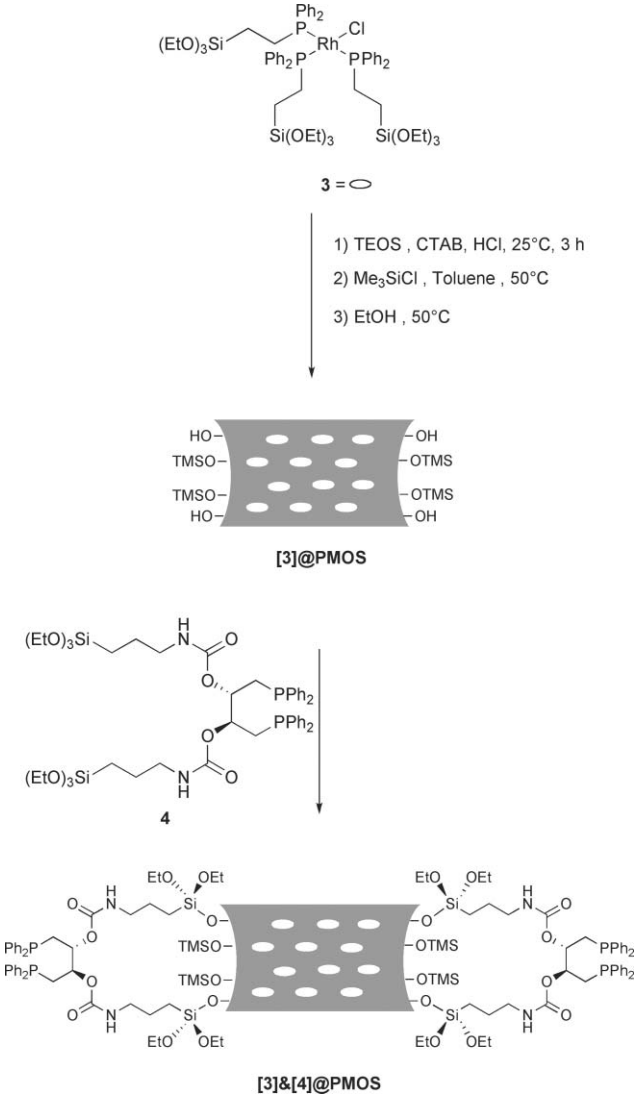

Scheme 3 Direct incorporation of achiral rhodium complex **3** into the walls of mesostructured SBA-3 type silica and subsequent functionalization of the pores with chiral auxiliary **4**.

d(100) spacing of 33.9 Å corresponding to 39.1 Å for the unit-cell parameter. The nitrogen adsorption-desorption isotherms for **[3]@PMOs** before and after the grafting of **4** were of type IV, characteristic of mesoporous materials (Fig. 6). **[3]@PMOs** displayed a high BET surface area of 1030 m^2g^{-1} with an average

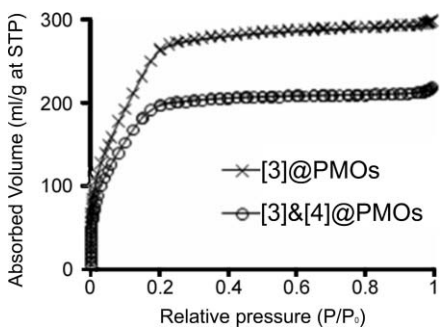

Fig. 6 Nitrogen adsorption/desorption isotherms of **[3]@PMOs** before and after the grafting of **4**.

pore diameter of 22 Å and a pore volume of 0.44 cm^3g^{-1} (Table 1). The relatively small pores diameter compared to that of **[2]/SBA-15** (22 Å *versus* 58 Å) originates from the synthesis conditions of the gel which used cetylammonium bromide as structure directing agent leading to the formation of a SBA-3 type silica material. The functionalization of this silica with **4** led to a decrease in the pore diameter (to 18 Å) as well as in surface area (to 800 m^2g^{-1}) and pore volume (to 0.33 cm^3g^{-1}), which is consistent with the presence of a significant amount of chiral auxiliary on the interior mesopore surfaces. It is also worth mentioning that the wall thickness in the SBA-3 type materials (21 Å for **[3][4]@PMOs**) was on average three times smaller than that of the SBA-15 solids (60 Å for **[2]/SBA-15**). We will see that this feature is of importance when considering possible interactions between the chiral directing group and the reactive rhodium site in **[3][4]@PMOs** (*vide infra*).

In the CP MAS ^{29}Si NMR spectra of **[3]@PMOs** and **[3][4]@PMOs** (Fig. 7), one observes discernable peaks at -45, -54 and -66 ppm (T^1, T^2 and T^3, respectively) confirming the formation of covalent bonds between organosilane and the surface. Peaks assignable to Q^2, Q^3, and Q^4 silicon sites of the silica framework (-87 to -107 ppm) were also observed in both spectra. Finally, the single resonance at 15.5 ppm typical of *M*-type (R_3-Si-(O-)) silicates was attributed to the trimethylsilyl capped silanol groups.

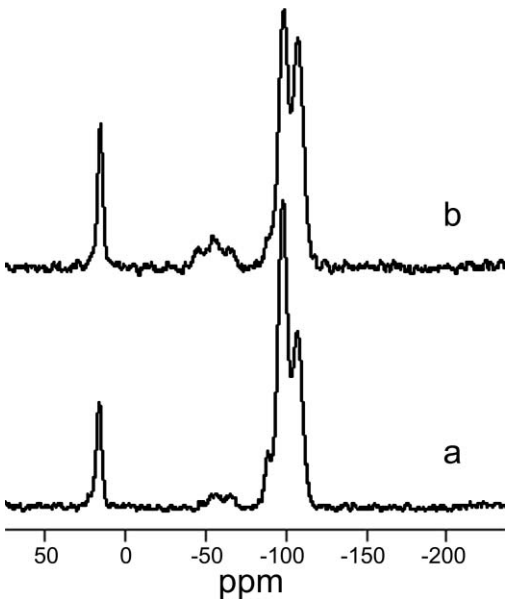

Fig. 7 CP-MAS ^{29}Si NMR of **[3]@PMOs** (a) and **[3][4]@PMOs** (b).

The ^{31}P NMR spectrum of **[3]@PMOs** exhibited an intense resonance at 40.5 ppm, attributed to rhodium-coordinated phosphine (Fig. 8a). As had been previously observed, the nature of the Rh-P bond in $RhCl\{PPh_2(CH_2)_2Si(OCH_2CH_3)_3\}_3$ seems unaffected by the inclusion of the complex into the hybrid matrix.[17] Subsequent functionalization of the pores with **4** led only to a slight shift of the signal to a higher magnetic field (to 37 ppm, Fig. 8b). Although one may discern a very weak resonance around δ -23.4 corresponding to free chiral diphosphine **4** (ESI, Figure S5),† these results suggest that most of the phosphorous atoms in **4** are in interaction with the

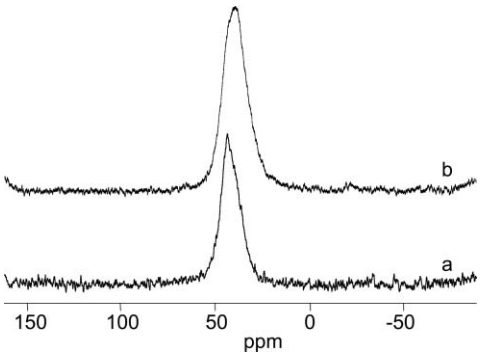

Fig. 8 MAS ^{31}P NMR of **[3]@PMOs** (a) and **[3][4]@PMOs** (b) (spinning rate 25 kHz).

rhodium centre and that ligand exchange has occurred between the $RhCl\{PPh_2(CH_2)_2Si(OCH_2CH_3)_3\}_3$ embedded in the walls of the silica framework and the DIOP immobilized in the pores. Recall that the walls of **[3]@PMOs** are relatively thin (17 Å) and that this type of catalytic solids have already demonstrated their capability to perform catalytic hydrogenation reactions and, hence, the metal site has been shown to be accessible.[17]

Elemental analysis of phosphorous and rhodium were obtained for both rhodium containing materials and are summarized in Table 1. **[3]@PMOs** was found to contain 0.8%$_{wt}$ Rh and 0.9%$_{wt}$ P (P/Rh ~ 3.5), suggesting that the integrity of the molecular precursor **3** was maintained throughout the synthesis. After the grafting of **4**, a molar ratio P/Rh of 4. 7 (0.8%$_{wt}$ Rh and 1.2%$_{wt}$ P) was found for **[3][4]@PMOs**, indicating approximately that an average of one DIOP ligand per rhodium atom was present on the surface.

Catalysis and recycling

These new Rh-materials were evaluated in the asymmetric hydrogenation of methyl (*Z*)-2-*N*-acetylaminocinnamate, which is a well known standard reaction (Scheme 4). The DIOP ligand was chosen for its *modest* enantiodiscrimination for this asymmetric hydrogenation, generally around 60%,[3,19] which would allow the observation of subtle effects the heterogenization has on performance. The hydrogenation reactions were performed in isopropanol catalyzed with 1.0% molar of Rh-catalyst, under different hydrogen pressures (5 and 10 bar) at different temperatures (25 or 40 °C). Results are summarized in Table 2. It was verified that an analogous silica containing no rhodium complex exhibited no measurable activity toward hydrogenation under standard conditions (40 °C, 10 bar H_2).

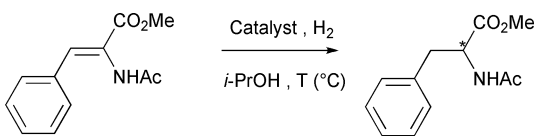

Scheme 4 Rhodium catalyzed hydrogenation of methyl (*Z*)-2-*N*-acetylaminocinnamate.

In a first series of experiments, we examined the performance of **[2]/SBA-15** formed after immobilization of neutral Rh-complex **2** in the pores of the SBA-15 type silica. Under 5 bar of hydrogen at 25 °C, full conversion and selectivity in the hydrogenated product were achieved after 72 hours of reaction, with an ee of 57% in favor of the (*R*)-enantiomer (Table 2, entry 1). To compare with the results reported by H. B. Kagan *et al.*[3] in homogeneous catalysis (substrate/Rh = 150, yield 90%, optical yield 55%), our heterogeneous system exhibited a lower activity but a similar enantioselectivity. In order to increase the activity, the temperature of hydrogenation reaction was raised to 40 °C (Table 2, entry 2). Quantitative conversion was observed after 48 hours, but this improvement was made at the expense of the enantioselectivity, which dropped to 22%.

Given that cationic Rh-complexes generally exhibit higher activity than neutral rhodium analogs, **[2]/SBA-15** was reacted with a large excess of $AgBF_4$ just prior to the catalysis. After removal of the excess of $AgBF_4$, the enamide was introduced in the reactor and the obtained cationic catalyst was then evaluated under the same last conditions (40 °C, 5 bar H_2). As expected, the rate of hydrogenation increased significantly and full conversion was observed after 24 hours, with an ee of 35% (Table 2, entry 3).

To prevent undesirable interactions between the highly reactive cationic metal centre and residual silanol groups, the hybrid material **[2]/SBA-15** was reacted with chlorotrimethylsilane. A clean replacement of the acidic proton of silanols by trimethyl silyl groups yielded the highly ordered material **[2S]/SBA-15** (ESI, Figure S4).† A cationic catalyst was derived from **[2S]/SBA-15** as described above. No major change in activity was noticed as full conversion was achieved in 24 hours, whereas enantioselectivity increased from 35 to 45% (Table 2, entry 4). This enhancement in asymmetric induction could be ascribed to the higher hydrophobicity of the nanopore environment.[20]

The importance of the proximity of the different elements constituting the heterogeneous chiral catalyst is evident in the

Table 2 Hydrogenation of methyl (*Z*)-2-*N*-acetylaminocinnamate catalyzed by **2** functionalized SBA-15 and **3** & **4** functionalized SBA-3 hybrid materials

Entry	Sample	$AgBF_4$	P_{H2} (bar)	Temp. (°C)	Time (hours)	Conv. (%)[a]	Yield (%)[a]	e.e. (%)[b]
1	**[2]/SBA-15**	—	5	25	72	100	84	57 (*R*)
2	**[2]/SBA-15**	—	5	40	48	100	100	22 (*R*)
3	**[2]/SBA-15**	2.3 eq.	5	40	24	100	100	35 (*R*)
4	**[2S]/SBA-15**	2.3 eq.	5	40	24	100	98	45 (*R*)
5	**[3][4]@PMOs**	—	5	25	120	15	13	26 (*R*)
6	**[3][4]@PMOs**	—	10	40	120	41	35	22 (*R*)
7	**[3]@PMOs**	—	10	40	120	10	—	0

[a] Conversions based on unreacted methyl (*Z*)-2-*N*-acetylaminocinnamate and yields were determined by GC with an internal standard (diethylene glycol di-*n*-butyl ether); [b] determined by HPLC using a chiral column.

case of material **[3||4]@PMOs**. Compared to **[2]/SBA-15**, the stereogenic and reactive centers in **[3||4]@PMOs** were not linked directly together, the chiral ligand derived from DIOP being grafted onto the surface of the pores and the achiral metallic center located in the walls of the silica matrix.

When the catalytic test reaction was performed in the presence of **[3||4]@PMOs** at 5 bar of hydrogen and at 25 °C, a low conversion of 15% was obtained after 120 hours, with an enantiomeric excess of 26% in favor of the (*R*)-enantiomer (Table 2, entry 5). Increasing the hydrogen pressure (to 10 bar) and the temperature (to 40 °C) resulted in a higher conversion of 41% and a slightly lower ee of 22% (Table 2, entry 6). Note that the material **[3]@PMOs** before functionalization with the DIOP-based compound was evaluated. A very low conversion (10%) with no enantioselectivity was achieved after 120 hours at 40 °C under 10 bar of hydrogen (Table 2, entry 7). The relatively low activity observed for both hybrids could stem from a restricted accessibility to the catalytic rhodium site, which is embedded within the silica framework. The observation of enantioinduction for **[3||4]@POMs** requires that the added DIOP ligand is in interaction with the product in formation, probably by coordination to the rhodium center (ligand exchange). In this context, one could also suppose that the chiral environment at the surface of the silica matrix due to the presence of the grafted DIOP ligand is sufficient to significantly induce a preferential orientation of the olefin with respect to the metal center fixed in the pore wall, leading to enantioselectivity.

Considering that catalyst stability and reusability was of primal interest, a preliminary study of the performance of **[2]/SBA-15** over several batch reaction cycles was undertaken. At the end of the reaction, **[2]/SBA-15** was allowed to settle for 2 hours and the reaction mixture was withdrawn *via* syringe. The catalytic solid was then washed with ethylacetate and reused without further purification by introducing to the reactor fresh substrate, solvent and hydrogen. The recycling process was repeated four times without significant loss of activity and enantioselectivity: full conversions were observed with yields in isolated hydrogenated product ranging from 84 to 87%, and ees in favor of the (*R*)-enantiomer varying between 49 and 57%. These results indicate that **[2]/SBA-15** is relatively robust under our reaction conditions and that no metal and no ligand leaching occurred from the surface of silica.

Conclusions

Two methods have been developed to prepare asymmetric heterogeneous catalysts involving the covalent tethering of catalyst elements to the silica matrix. In one case, a chiral metal complex was tethered to the pore wall of a SBA-15 mesoporous silica *via* an achiral phosphine ligand. In the other approach, the metal was embedded into the silica matrix and the chiral auxiliary was grafted into the pores of the resultant inorganic-organometallic hybrid material.

Reasonable catalyst performances, both in terms of activity, selectivity and enantioselectivity were demonstrated for each of these materials. Finally, the directly tethered catalyst was recycled four times without significant degradation of catalyst performance.

Experimental

General

All manipulations were conducted under a strict inert atmosphere or vacuum conditions using Schlenk techniques including the transfer of the catalysts to the reaction vessel. The solvents were dried using standard methods and stored over activated 4 Å molecular sieves. Tetraethoxysilane (TEOS), poly(ethyleneoxide)-poly(propyleneoxide)-poly(ethyleneoxide) block copolymer (Pluronic 123, Mw: 5000) were purchased from Aldrich Chemical and used without further purification. Cetyltrimethylammonium bromide (CTAB) and and (-)-2,2-dimethyl-4,5-bis[(diphenylphosphino)methyl]-1,3-dioxolane (DIOP) were obtained from Acros. 2-(Diphenylphosphino)-ethyl-triethoxysilane was purchased from ABCR and chloro-(1,5-cyclooctadiene)rhodium (I) dimer from Alfa Aesar. The transition metal precursor, $RhCl\{PPh_2(CH_2)_2Si(OCH_2CH_3)_3\}_3$ (**3**), was prepared by reacting chloro(1,5-cyclooctadiene)rhodium dimer with 3 equivalents of $PPh_2(CH_2)_2Si(OCH_2CH_3)_3$, according to the procedure reported by Kröcher *et al.*[21] The synthesis of (2S,3S)-1,4-bis(diphenylphosphino)butane-2,3-diyl-bis[(3-triethoxysilyl) propyl)carbamate] (**4**) was achieved through the hydrolysis of the diop ligand with perchloric acid to produce the disphosphine diop-diol, (-)-1,4-bis(diphenylphosphino)butane-2,3-diol, followed by reaction of the free hydroxyl groups with (3-isocyanatopropyl)triethoxysilane.

Low-angle X-ray powder diffraction (XRD) data were acquired on a Bruker D5005 diffractometer using Cu Kα monochromatic radiation (λ = 1.054184 Å). Nitrogen adsorption–desorption isotherms at 77 K were measured using a Micromeritics ASAP 2010M physisorption analyzer. The samples were evacuated at 160 °C for 24 h before the measurements. Specific surface areas were calculated following the BET procedure. Pore size distribution was obtained by using either the BJH pore analysis applied to the desorption branch of the nitrogen adsorption/desorption isotherm or the BdB pore analysis. Infrared spectra were recorded from KBr pellets using a Mattson 3000 IRFT spectrometer. A Netzsch thermoanalyser STA 409PC was used for simultaneous thermal analysis combining thermogravimetric (TGA) and differential thermoanalysis (DTA) at a heating rate of 10 °C min^{-1} in air from 25–1000 °C. Solid state NMR spectra were recorded on a BRUKER AVANCE-300 spectrometer using 4 mm diameter ZrO_2 rotors. ^{13}C NMR spectra (75.49 MHz) were obtained with a standard 1D CPMAS ^{13}C - ^{1}H sequence with a spin rate of 12000 Hz to remove the chemical shift anisotropy and, thus, the side-bands from the 0–200 ppm region (contact time: 2 ms, recycle time: 10 s). For the ^{31}P NMR spectra (121.53 MHz), a pulse length of 2 μs with a recycle time of 20 s was used. The spinning rate was 10000 Hz or 25000 Hz depending on the samples and the chemical shifts are given relative to an external 85% H_3PO_4. The ^{29}Si MAS spectra (59.64 MHz) were recorded by using a pulse length of 3 μs, a contact time of 3.5 ms and a recycle time of 10 s. The spinning rate was 10000 Hz and the chemical shifts are given relative to TMS. CP MAS ^{29}Si solid NMR measurements were collected on a Bruker DSXv400 spectrometer at a frequency operating at 79.49 MHz. A 5 ms (y=p/2) pulse was used with a repetition time of 80 s.

Liquid NMR spectra were recorded on a Bruker AC-300 spectrometer and referenced as following: ^{1}H (300 MHz), internal $SiMe_4$ at $\delta = 0.00$ ppm, ^{13}C (75 MHz), internal $CDCl_3$ at $\delta = 77.2$ ppm, and ^{31}P (121 MHz), external 85% H_3PO_4 at $\delta = 0.00$ ppm. Metal determinations were performed by ICP-OES (Activa Jobin Yvon) spectroscopy from a solution obtained by treatment of the solid catalyst with a mixture of HF, HNO_3 and H_2SO_4 in a Teflon reactor at 150 °C. Flash chromatography was performed under nitrogen at a pressure slightly greater than atmospheric pressure using silica (Merck Silica Gel 60, 230 - 400 mesh). Thin layer chromatography was performed on Merck Silica Gel 60 F_{254}.

GC analyses were performed on a Varian CP-3800 gas chromatograph equipped with a flame ionization detector, a Varian CP-8400 autosampler and a CP-Sil5CB capillary column (30 m, 0.32 mm internal diameter, 0.25 μm film thickness). Nitrogen was used as gas carrier. Optical rotations were recorded using a Perkin–Elmer 241 polarimeter. Enantiomeric excess was determined by HPLC with a Chiralpak^{AD} column (25 cm × 4.6 mm) using a 90/10 ratio of hexane/*i*-propanol as eluent.

Chloro{diphenyl[2(triethoxysilyl)ethyl]phosphino}{(-)-2,2-dimethyl-4,5-bis[(diphenylphosphino)methyl]-1,3-dioxolane} rhodium (2)

2-(triethoxysilyl)ethyl)diphenylphosphine (0.45 g, 1.2 mmol) dissolved in 5 mL of dry and degassed toluene was added to a solution of $[Rh(COD)Cl]_2$ (0.29 g, 0.60 mmol) in degassed toluene (5 mL). The reaction mixture was stirred at room temperature for 3 hours followed by dropwise addition of a solution of diop (0.60 g, 1.2 mmol) in toluene (10 mL). At completion, monitored by ^{31}P NMR spectroscopy, the reaction mixture was used without further purification for the immobilization on mesoporous materials.

^{31}P NMR (81 MHz, C_6D_6) δ 30.1 (ddd, 1P, $^{1}J_{(P(1)-Rh)} = 185.7$ Hz, $^{2}J_{(P(1)-P(2))} = 40.5$ Hz, $^{2}J_{(P(1)-P(3))} = 45.4$ Hz, P_1 of diop ligand), 24.9 (ddd, 1P, $^{2}J_{(P(2)-P(3))} = 359.8$ Hz, $J_{(P(2)-Rh)} = 138.3$ Hz, $^{2}J_{(P(2)-P(1))} = 40.5$ Hz, P_2 of diop ligand), 11.3 (ddd, 1P, $^{2}J_{(P(3)-P(2))} = 359.8$ Hz, $J_{(P(3)-Rh)} = 137.6$ Hz, $^{2}J_{(P(3)-P(1))} = 45.5$ Hz, P_3 of 2-(triethoxysilyl)ethyl)diphenylphosphine).

Synthesis of hybrid silica materials

Post-functionalization. Mesoporous SBA-15 type silica was used as support and was prepared by the acid catalyzed, non-ionic assembly pathway described by Margolese *et al.*[22] The structure directing agent (Pluronic 123) was removed quantitatively from the as-synthesized material by calcination at 500 °C overnight under air as evidenced by TGA analysis and infrared spectroscopy. Prior to the grafting reaction, the surfactant-free mesoporous silica was rigorously dried under a flow of nitrogen at 200 °C. (**2**) (1.2 g, 1.2 mmol) Dissolved in 20 mL of deaerated toluene was then added to a suspension of SBA-15 silica (1 g) in dry toluene. The reaction mixture was stirred at 25 °C for two hours to allow the diffusion of the molecular precursor into the channels of the pores. The reaction mixture was then heated at 65 °C overnight. The resulting solid was filtered under nitrogen, washed thoroughly with a small amount of toluene and finally dried at 30 °C under vacuum, **[2]/SBA-15** (ICP-AES analysis: P, 2.5%wt; Rh, 2.4%wt). In some cases, the silica surface was further capped using $(CH_3)_3SiCl$ as silylating agent, **[2S]/SBA-15**. The cationic analogues of these latter were prepared *in situ* just prior to catalysis by reacting either **[2]/SBA-15** or **[2S]/SBA-15** with a slight excess of $AgBF_4$ according to procedures previously described in the literature.[23]

One-pot integrated approach. The synthesis of periodic mesoporous organosilica with bridging organophosphine rhodium complexes in the pore walls was recently reported by one of the authors.[17] The synthesis of the hybrid material was achieved in three steps using the following molar composition: TEOS, 1; H_2O, 120; CH_3CN, 4.3; HCl, 9.2; CTAB, 0.12. When $RhCl\{PPh_2(CH_2)_2Si(OCH_2CH_3)_3\}_3$ (**3**) was used, the calculation of the molar composition was based on the total number of condensable silicon centers, from TEOS and the rhodium complex. In a typical procedure, CTAB was first dissolved in water, HCl and half of the amount of acetonitrile used in the gel composition. TEOS was then prehydrolyzed for 15 minutes at room temperature prior to the addition of (**3**) solubilized in the remaining portion of acetonitrile. The reaction mixture was stirred for 3 h at room temperature. The solid product was recovered by filtration, washed with water and dried under vacuum overnight at 25 °C. The silylation and extraction steps were carried out as described in ref. 17, leading to the achiral hybrid material **[3]@PMOs** (ICP-AES analysis: P, 0.88%wt; Rh, 0.82%wt). The chirality was introduced subsequently *via* the functionalization of the void space, left unoccupied after template removal, with (2S,3S)-1,4-bis(diphenylphosphino)butane-2,3-diyl-bis[(3-triethoxysilyl) propyl)carbamate] (**4**).[18] The obtained material, **[3][4]@PMOs**, provides a new type of catalyst in which the metallic center and the chiral auxiliary are not linked together but rather placed in different microenvironments in the catalytic solid (ICP-AES analysis: P, 1.18%wt; Rh, 0.76%wt).

Catalytic test

The catalytic reactions were carried out in a high pressure stainless steel autoclave (Parr-Equilabo, 300 mL) fitted with a glass liner, temperature regulator and a valve to allow direct sampling of the reaction mixture. Conversion and yield were determined by GC based on relative area of the GC-signals referred to an internal standard (diethylene glycol di-*n*-butyl ether) calibrated to the corresponding pure compounds.

In a typical procedure, the hybrid catalyst (1.14×10^{-2} mmol of Rh based on elemental analysis) was first evacuated at 40 °C during 4 hours to remove physisorbed water and then suspended in 5 mL of isopropanol. In the mean time, a solution composed of 0.25 g (1.14 mmol) of methyl (*Z*)-2-*N*-acetylaminocinnamate,[24] 0.05 g (0.24 mmol) of diethylene glycol di-*n*-butyl ether (internal standard) and 18 mL of degassed isopropanol was prepared and transferred onto the catalytic suspension. The autoclave, containing a magnetic stirring bar, was then charged with the reaction mixture under a nitrogen atmosphere. The autoclave was sealed, flushed first with nitrogen (7 bar) and then with hydrogen (10 bar) by repeated pressurization and release, and then pressurized with the desired hydrogen pressure. The temperature was then adjusted to the desired value. The reaction was monitored by GC until completion of the reaction. At the end of the reaction, the autoclave was opened and the solution filtered through a celite pad. After removal of the solvent under

reduced pressure, the reaction products were analyzed by HPLC on a chiral column to determine the enantiomeric excess.

Recycling procedure

In the recycling studies, fresh catalyst was used as for a standard catalytic run. Stirring and heating were then removed and the supernatant was carefully withdrawn with a syringe. The catalyst was washed three time with ethylacetate, dried, weighed carefully and reused for another catalytic run.

Acknowledgements

RS thanks the French Ministry of Education for a fellowship.

Notes and references

1 (*a*) H-U. Blaser, *Chem. Commun.*, 2003, 293–296; (*b*) N. B. Johnson, I. C. Lennon, P. H. Moran and J. A. Ramsden, *Acc. Chem. Res.*, 2007, **40**, 1291–1299; (*c*) J-P. Genet, *Pure Appl. Chem.*, 2002, **74**, 77–83; (*d*) *Asymmetric Catalysis on Industrial Scale: Challenges, Approaches and Solutions*, H-U. Blaser, and E. Schmidt, Eds; Wiley-VCH, Weinheim, 2004.

2 (*a*) W. S. Knowles, M. J. Sabacky and B. D. Vineyard, *Chemtech*, 1972, **2**, 590–591; (*b*) W. S. Knowles, *Angew. Chem., Int. Ed.*, 2002, **41**, 1998–2007.

3 H. B. Kagan and T-P. Dang, *J. Am. Chem. Soc.*, 1972, **94**, 6429–6433.

4 (*a*) W. S. Knowles, M. J. Sabacky and B. D. Nineyard, *J. Chem. Soc., Chem. Commun.*, 1972, 10–11; (*b*) B. D. Vineyard, W. S. Knowles, M. J. Sabacky, G. L. Bachman and D. J. Weinkauff, *J. Am. Chem. Soc.*, 1977, **99**, 5946–5952.

5 M. D. Fryzuk and B. Bosnich, *J. Am. Chem. Soc.*, 1977, **99**, 6262–6267.

6 (*a*) M. J. Burk, J. E. Feaster and R. L. Harlow, *Organometallics*, 1990, **9**, 2653–2655; (*b*) M. J. Burk, *J. Am. Chem. Soc.*, 1991, **113**, 8518–8519; (*c*) M. J. Burk, J. E. Feaster, W. A. Nugent and R. L. Harlow, *J. Am. Chem. Soc.*, 1993, **115**, 10125–10138; (*d*) M. J. Burk, J. R. Lee and J. P. Martine, *J. Am. Chem. Soc.*, 1994, **116**, 10847–10848; (*e*) M. J. Burk, Y. M. Wang and J. R. Lee, *J. Am. Chem. Soc.*, 1996, **118**, 5142–5143.

7 (*a*) A. Miyashita, A. Yasuda, H. Takaya, K. Toriumi, T. Ito, T. Souchi and R. Noyori, *J. Am. Chem. Soc.*, 1980, **102**(27), 7932–7934; (*b*) A. Miyashita, H. Takaya, T. Souchi and R. Noyori, *Tetrahedron*, 1984, **40**, 1245–1253; (*c*) H. Takaya, K. Mashima, K. Koyano, M. Yagi, H. Kumobayashi, T. Takemomi, S. Akutagawa and R. Noyori, *J. Org. Chem.*, 1986, **51**, 629–635.

8 (*a*) P. McMorn and G. J. Hutchings, *Chem. Soc. Rev.*, 2004, **33**, 108–122; (*b*) M. Heitbaum, F. Glorius and I. Escher, *Angew. Chem., Int. Ed.*, 2006, **45**, 4732–4762; (*c*) C. E. Song and S.-G. Lee, *Chem. Rev.*, 2002, **102**, 3495–3524; (*d*) Z.-L. Lu, E. Lindner and H. A. Mayer, *Chem. Rev.*, 2002, **102**, 3543–3578; (*e*) A. P. Wight and M. E. Davis, *Chem. Rev.*, 2002, **102**, 3589–3614; (*f*) D. E. De Vos, M. Dams, B. F. Sels and P. A. Jacobs, *Chem. Rev.*, 2002, **102**, 3615–3640.

9 (*a*) F. M. de Rege, D. K. Morita, K. C. Ott, W. Tumas and R. D. Broene, *Chem. Commun.*, 2000, 1797–1798; (*b*) H. H. Wagner, H. Hausmann and W. F. Hölderich, *J. Catal.*, 2001, **203**, 150–156; (*c*) W. P. Hems, P. McMorn, S. Riddel, S. Watson, F. E. Hancock and G. J. Hutchings, *Org. Biomol. Chem.*, 2005, **3**, 1547–1550; (*d*) C. Simons, U. Hanefeld, I. W. C. E. Arends, R. A. Sheldon and T. Maschmeyer, *Chem.–Eur. J.*, 2004, **10**, 5829–5835.

10 R. Augustine, S. Tanielyan, S. Anderson and H. Yang, *Chem. Commun.*, 1999, 1257–1258.

11 S. A. Raynor, J. M. Thomas, R. Raja, B. F. G. Johnson, R. G. Bell and M. D. Mantle, *Chem. Commun.*, 2000, 1925–1926.

12 C. M. Crudden, D. Allen, M. D. Mikoluk and J. Sun, *Chem. Commun.*, 2001, 1154–1155.

13 I. Steiner, R. Aufdenblatten, A. Togni, H.-U. Blaser and B. Pugin, *Tetrahedron: Asymmetry*, 2004, **15**, 2307–2311.

14 A. R. McDonald, C. Müller, D. Vogt, G. P. M. van Klink and G. van Koten, *Green Chem.*, 2008, **10**, 424–432.

15 H. Brunner, C. Zettler and M. Zabel, *Z. Anorg. Allg. Chem.*, 2003, **629**, 1131–1135.

16 The silica content refers to residual mass at 1000 °C. For the purposes of calculation, rhodium is supposed to remain on the solid in the form of RhxOy.

17 V. Dufaud, F. Beauchesne and L. Bonneviot, *Angew. Chem., Int. Ed.*, 2005, **44**, 3475–3477.

18 (**4**) Was obtained by chemical modification of DIOP ligand through a reaction sequence consisting of hydrolysis and condensation with organosiloxane precursor. Detailed synthesis of (**4**) is fully described in another report submitted to *J. Mol. Catal. A: Chem.*

19 (*a*) W. Hu, C.-C. Chen, G. Xue and A. S. C. Chan, *Tetrahedron: Asymmetry*, 1998, **9**, 4183–4192; (*b*) F. Robert, G. Oehme and D. Sinou, *J. Mol. Catal. A: Chem.*, 1999, **139**, 105–108; (*c*) W. Li and X. Zhang, *J. Org. Chem.*, 2000, **65**, 5871–5874.

20 H. Zhang and C. Li, *Tetrahedron*, 2006, **62**, 6640–6649.

21 O. Kröcher, R. A. Köppel, M. Fröba and A. Baiker, *J. Catal.*, 1998, **178**, 284–298.

22 D. Margolese, J. A. Melero, S. C. Christiansen, B. F. Chmelka and G. D. Stucky, *Chem. Mater.*, 2000, **12**, 2448–2459.

23 (*a*) R. R. Schrock and J. A. Osborn, *J. Am. Chem. Soc.*, 1971, **93**, 2397–2407; (*b*) D. Moulin, C. Darcel and S. Jugé, *Tetrahedron: Asymmetry*, 1999, **10**, 4729–4743.

24 A. Kawazaki, K. Maekawa, K. Kubo, T. Igarashi and T. Sakurai, *Tetrahedron*, 2004, **60**, 9517–9524.

